Mechanical response of smectic-*C* elastomers

J. M. Adams and M. Warner
Cavendish Laboratory, JJ Thomson Avenue, Cambridge CB3 0HE, United Kingdom
(Received 10 October 2007; published 8 February 2008)

The elastic response of a smectic-*C* elastomer to three deformations, namely imposed λ_{xx}, λ_{xz}, and λ_{zz}, has been modeled using a nonlinear theory of a nematic elastomer with embedded smectic layers, and with the director tilt (in the **x** direction) at a fixed angle with respect to the smectic layer normal (**z** direction). The main focus is the elastic response after any soft mode of the sample. It is found that the elastomer contracts in the **x** direction under λ_{xz} shear. On stretching parallel to the layer normal it is found that there is a soft mode that acts to rotate the director toward the **z** direction. The deformation of the system after this soft mode can be reduced to shear and elongation in the plane of the layers. We make predictions of the mechanical response of the elastomer, in particular the length of the soft plateau and the asymptotic modulus for the elastomer when stretched parallel to the layer normal. Finally, since monodomain Sm-*C* elastomers are made by the deformation-induced alignment of polydomains, we describe these important systems. Qualitative behavior of the model is then compared to existing experimental literature on the mechanical alignment of polydomains

DOI: 10.1103/PhysRevE.77.021702 PACS number(s): 61.30.−v, 83.80.Va, 42.70.Df

I. INTRODUCTION

Liquid crystal elastomers (LCEs) are polymer networks formed by crosslinking liquid crystalline polymers. These polymers are typically connected to rigid rodlike molecules that distort the conformation of the polymer; for example, if the rods are in the nematic phase then the conformation of the polymer backbones is anisotropic. The large bulk modulus of these elastomers in comparison to their shear modulus dictates that they are volume conserving. They display several remarkable properties, such as soft elasticity which will concern us here. Soft elasticity refers to the ability of LCEs to deform at no energy cost, and arises because the deformation can be performed by rotation of the director, and consequently the anisotropic shape distributions of the polymers [1–3].

Smectic liquid crystal elastomers are composed of liquid crystalline polymers that form the layered smectic phase. It differs from the nematic phase in that it has a very large modulus, B associated with the distortion of the layer spacing. These elastomers display highly anisotropic properties because the layer modulus is much larger than the shear modulus of the polymer network. There are a large number of smectic liquid crystal phases, and the corresponding elastomers display a wide variety of elastic properties. Smectic-*A* (Sm-*A*) elastomers have their director along their layer normal and have been shown both experimentally [4], and theoretically [5,6] to behave as 2D rubbers when stretched in the plane, whereas when stretched parallel to the plane normal they initially have an extremely high elastic modulus B. After the strain passes a critical threshold the elastic modulus falls to $r\mu$. By contrast smectic-*C* (Sm-*C*) elastomers have their director at a fixed angle to their layer normal and are believed to be elastically soft when suitably deformed [7–9]. For example when a negative xz shear is applied to an Sm-*C* elastomer initially with its layer normal in the **z** direction, and the in-plane projection of its director in the **+x** direction, it can be softly deformed as shown in Fig. 1. The director rotates on a cone about **z**, the unchanging direction of the layer normal. There are accompanying shears λ_{xy} and λ_{yz} as the rotation proceeds. For the case of imposed λ_{xz} the rotation of the director is complete for $\lambda_{xz}=-(r-1)\sin 2\theta/\rho$. Here r is the anisotropy of the polymer chains, θ is the tilt of the director, and $\rho=\sin^2\theta+r\cos^2\theta$. When the rotation is complete, $\lambda_{xy}=0$. Important work has been carried out on the mechanical properties of partially alligned Sm-*C* samples. The first experiments [10] were on elastomers with aligned layers but where the director tilts either parallel or antiparallel to the direction of in-plane stretch imposed at second-stage crosslinking. Later experiments [11] were on samples where the director has a common direction, but layer normals take two directions thereby forming a chevron structure. When strains are imposed perpendicular to the director, it reorients to accommodate the shape change. The corresponding stress-strain relation changes slope when rotation occurs showing that as in nematic elastomers, mechanical properties are profoundly influenced by the redirection of nematic order.

Experimental work on spontaneous distortions in Sm-*C* elastomers related to the shape changes of Fig. 1 has been

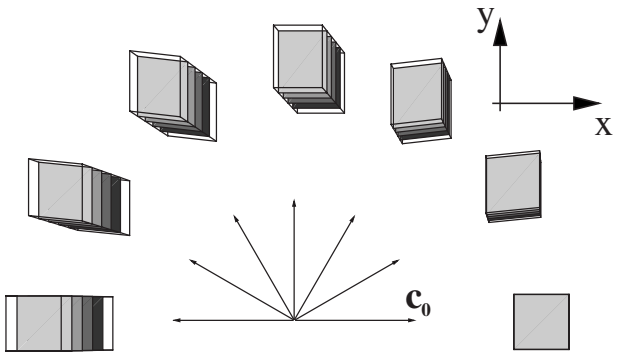

FIG. 1. Soft mode of an Sm-*C* elastomer as it is sheared. The component of the director perpendicular to the layer normal rotates as the soft mode is performed, as illustrated by the vector **c** shown. $\mathbf{c}_0$ marks the initial direction of **c**.

carried out, for example a Sm-*C* monodomain can be heated to the Sm-*A* phase, and undergoes a spontaneous shear distortion that is reversible on cooling back to the Sm-*C* phase [12]. Theoretically the mechanical properties of a monodomain could exhibit soft elasticity even when the macroscopic deformation applied is not one of the pure soft modes allowed by symmetry. But in that case soft elasticity is accompanied by microstructure formation that results in a wider set of deformations that are also soft [13]. Understanding how the director and the layer normal respond to an imposed deformation gradient in Sm-*C* elastomers are key to understanding how the elastomer deforms. The competing requirements of conserving the layer spacing and reorienting the director to accommodate the imposed deformation gradient result in sympathetic shears. This picture is complicated by the presence of boundary conditions at the clamps that result in a complicated mix of deformation gradients.

The aim of this paper is to study the response of a Sm-*C* elastomer beyond soft deformations. The effect of constraining boundaries, responsible for the formation of microstructure, is ignored, instead focusing on the physics of the monodomain deformation. The effect of three different deformations applied to a monodomain, chosen to have a nonsoft response, are considered. Comparison is then made to experimental literature by considering the alignment of polydomain samples.

II. FREE ENERGY DENSITY IN SMECTIC-*C* ELASTOMERS

To model Sm-*C* elastomers the following free energy will be used [5,9]

$$f = \tfrac{1}{2}\mu \,\mathrm{Tr}[\underline{\underline{\lambda}} \cdot \underline{\underline{\ell}}_0 \cdot \underline{\underline{\lambda}}^T \cdot \underline{\underline{\ell}}^{-1}] + \tfrac{1}{2}B(d/d_0 - 1)^2, \qquad (1)$$

where μ is the rubber modulus, and B is the smectic layer modulus. The first term is that of a rubber with only the underlying nematic rubber free energy. The second is the cost of changing the layer spacing from its equilibrium value, d_0. The mean square distribution of the Gaussian polymer chains is described by the step length tensor $\underline{\underline{\ell}} = \underline{\underline{\delta}} + (r-1)\mathbf{nn}^T$. Experimentally, the value of $B/\mu \gg 1$ in $\overline{\overline{\mathrm{S}}}$m-*A* elastomers [14]; consequently our main focus is $B/\mu \to \infty$. It is also assumed that volume is conserved, i.e., $\det(\underline{\underline{\lambda}}) = 1$ as a consequence of the even larger bulk modulus of the rubber, K. Additionally we assume here that the tilt angle of the director with respect to the layer normal is rigidly fixed. The moduli are ordered as follows: $K \gg B \gg \mu$. In this model layers are anchored strongly in the matrix and thus deform affinely with it. The response of the layer normal, initially given by $\mathbf{k}_0$, to the imposed deformation gradient $\underline{\underline{\lambda}}$ is $\mathbf{k} = \underline{\underline{\lambda}}^{-T} \cdot \mathbf{k}_0 / |\underline{\underline{\lambda}}^{-T} \cdot \mathbf{k}_0|$. The accompanying layer spacing change is given by $d/d_0 = 1/|\underline{\underline{\lambda}}^{-T} \cdot \mathbf{k}_0|$, and the initial and current directors given by $\mathbf{n}_0$ and $\mathbf{n}$, respectively. The layer spacing expression along with $\det(\underline{\underline{\lambda}}) = 1$ for volume conservation, are both highly nonlinear and render Eq. (1) into a complicated form. Since the deformations are large the nonlinearities cannot be ignored and (1) has been shown to well describe the complex, nonlinear distortions of Sm-*A* elastomers [5]. The director and the layer normal are related by the tilt angle of the director, θ (typically $\lesssim 22°$). It is conventional to denote the direction of tilt by the unit vector $\mathbf{c}$ which is in the plane perpendicular to $\mathbf{k}$, i.e., $\mathbf{c} \cdot \mathbf{k} = 0$. The director is then given by

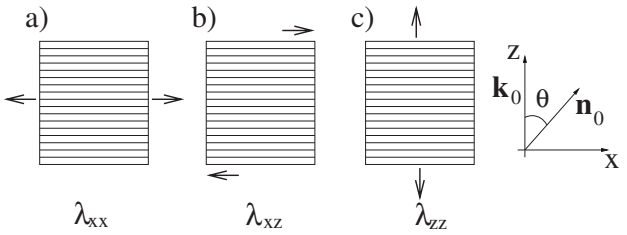

FIG. 2. Imposed deformation; (a) elongation perpendicular to the layer normal, (b) shearing perpendicular to the layer normal, and (c) elongation parallel to the layer normal.

$$\mathbf{n} = \mathbf{k}\cos\theta + \mathbf{c}\sin\theta. \qquad (2)$$

The free energy density has the free vector $\mathbf{c}$ to be minimized over. Mathematically it is awkward to do this minimisation in general because of the constraints on the direction $\mathbf{c}$, and the resulting Lagrange multipliers that must be calculated.

We show below how B and μ separately enter the free energy density, before eliminating the effect of changing layer spacing ($B \to \infty$). The main features of the Sm-*C* behavior can be exhibited in this limit of rigidly fixed layer spacing.

III. EXAMPLE DEFORMATIONS

Three examples of imposed deformation are now considered to develop an intuition for the elastic response as shown in Fig. 2. These three deformations were chosen to exhibit the responses of Sm-*C* elastomers to imposed deformation gradients, for their simplicity and for their experimental relevance. The uniaxial extension experiments have been performed on nematic elastomers, and the simple shear has been used in the alignment of Sm-*C* elastomers. The director orientation was chosen so as to, as far as possible, avoid any softness of the deformation. In the first two cases analysed here (imposed λ_{xx} and λ_{xz}) the layer normal remains fixed, simplifying calculation of the vector $\mathbf{c}$, as it must remain fixed in the xz plane. In the last case of imposed λ_{zz} the director and layer normal move, but its motion can be simplified. The axes used here are layer normal along the z axis and $\mathbf{c}$ initially pointing in the $\mathbf{x}$ direction.

A. Imposed λ_{xx}

This case is the simplest of the three illustrated in Fig. 2 and is analytic. The deformation gradient occurring as a result of the applied λ_{xx} deformation is upper triangular, as the director remains in the xz plane. Here the following deformation matrix will be used

$$\underline{\underline{\lambda}} = \begin{pmatrix} \lambda_{xx} & \lambda_{xy} & \lambda_{xz} \\ 0 & 1/(\lambda_{xx}\lambda_{zz}) & \lambda_{yz} \\ 0 & 0 & \lambda_{zz} \end{pmatrix}. \tag{3}$$

The orientation of the director remains fixed during deformations of the form of Eq. (3). This is consistent with the analysis of a Sm-*A* elastomer where the layer normal does not move when a strain perpendicular to the layer normal is applied. Consequently, the components λ_{xy} and λ_{yz} are zero. These assumptions were confirmed by a numerical minimization of the free energy density. Substituting in the resulting deformation tensor into the free energy density expression together with

$$\mathbf{n}_0 = \mathbf{n} = (\sin\theta, 0, \cos\theta) \tag{4}$$

produces the following

$$f = \tfrac{1}{2}\mu\left(\lambda_{xx}^2 + \frac{1}{\lambda_{zz}^2\lambda_{xx}^2} + \lambda_{zz}^2 + \frac{1}{r}\left[\rho\lambda_{xz} - \tfrac{1}{2}(\lambda_{zz} - \lambda_{xx})(r-1)\sin 2\theta\right]^2\right) + \tfrac{1}{2}B(\lambda_{zz}-1)^2, \tag{5}$$

where $\rho = \sin^2\theta + r\cos^2\theta$. The Poisson's ratios of a Sm-*C* elastomer can be obtained from this free energy expression by first minimising with respect to λ_{xz} and then calculating the small strain response in the **z** direction to an imposed **x** strain. The result is the same as the Sm-*A* case

$$\nu = \frac{B + 2\mu}{B + 4\mu}. \tag{6}$$

Experimentally it is observed that $B/\mu \gg 1$. In keeping with this it is now assumed that $\lambda_{zz}=1$ and Eq. (5) becomes (up to additive constants)

$$f = \tfrac{1}{2}\mu\left(\lambda_{xx}^2 + \frac{1}{\lambda_{xx}^2} + \frac{1}{r}\left[\rho\lambda_{xz} + \tfrac{1}{2}(\lambda_{xx}-1)(r-1)\sin 2\theta\right]^2\right). \tag{7}$$

On minimizing the free energy density Eq. (7) with respect to λ_{xz} the following is obtained:

$$\lambda_{xz} = -\frac{(r-1)(\lambda_{xx}-1)\sin 2\theta}{2\rho}. \tag{8}$$

Note that the sympathetic shear is of negative sign, i.e., it is in the opposite sense to the tilt of the director. In a nematic the opposite sign of shear (positive) would be expected as the director rotates toward the extension direction. Here the elongation in the **x** direction acts to extend the polymer chains, whereas the compensating *xz* shear reduces their extent, thus lowering the energy of the system, and resulting in a negative shear. An illustration of this is shown in Fig. 3.

Substituting the minimum values back into the free energy yields

$$f = \tfrac{1}{2}\mu\left(1 + \frac{1}{\lambda_{xx}^2} + \lambda_{xx}^2\right), \tag{9}$$

i.e., a 2D rubber elastic response, with an elastic modulus of 4μ, rather than the usual modulus against extension of 3μ.

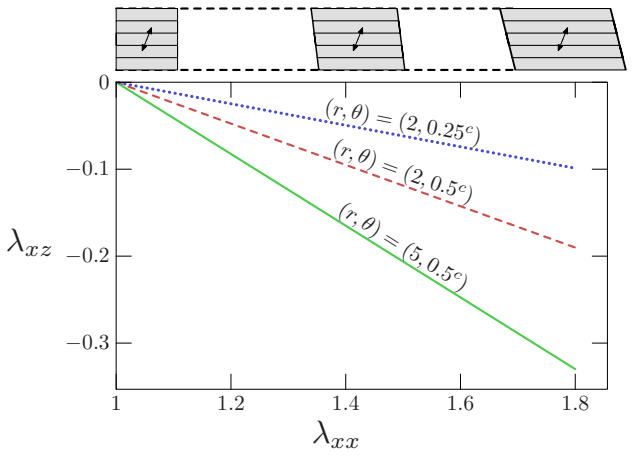

FIG. 3. (Color online) Sympathetic shear strains resulting from applying a uniaxial elongation in the **x** direction (lines labeled with the appropriate model parameters). An illustration of the elastomer is provided above the graph of the $(r,\theta)=(5,0.5^c)$ case.

Suppression by the layers of contraction along **z** means, since volume is constant, greater contraction along **y** and hence the extra energy.

This analysis is only valid for extensional deformations ($\lambda_{xx} > 1$). If the system were compressed, then theoretically it would be soft, because the director rotates around in the plane of the layers toward **y**, thereby shortening the elastomer's natural length in the direction of compression, see the first four frames of Fig. 1.

If this stretch is applied using two clamps to stretch the sample, then because of the sympathetic shear response microstructure will form. However, if it is not possible to form the required microstructure to allow the sympathetic shear, then the modulus of the sample will be different. If $\lambda_{xz}=0$ in Eq. (7) then the system is even stiffer than the corresponding 2D elastomer, with an elastic modulus $(\partial^2 f/\partial\lambda_{xx}^2|_{\lambda_{xx}=1})$ given by

$$\left(4 + \frac{(r-1)^2\sin^2 2\theta}{4r}\right)\mu. \tag{10}$$

The measurement of this modulus would provide an indication of whether the system is able to form the required microstructure to lower its elastic modulus.

B. Imposed λ_{xz}

This case has the same free energy expression as the imposed λ_{xx} case considered above. However, the sympathetic shears are now being driven by a different matrix element. As in the case above, the sympathetic shears will be a subset of those that occur during the soft mode because the director is now static. The deformation gradient tensor is taken to be of the form

$$\underline{\underline{\lambda}} = \begin{pmatrix} \lambda_{xx} & 0 & \lambda_{xz} \\ 0 & 1/\lambda_{xx} & 0 \\ 0 & 0 & 1 \end{pmatrix}. \tag{11}$$

The free energy density is the same as Eq. (7). Minimization with respect to λ_{xx} is required and results in a quartic equa-

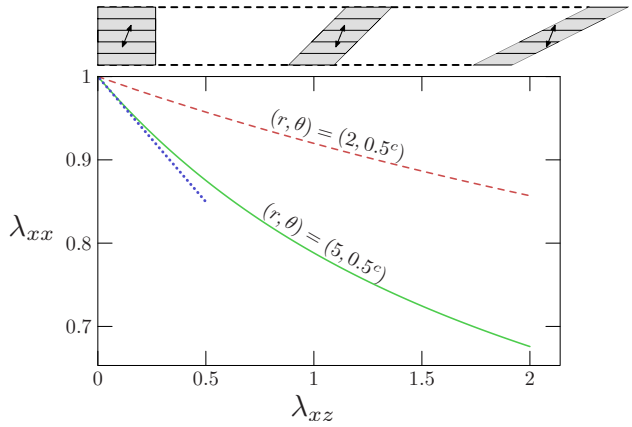

FIG. 4. (Color online) Sympathetic contractions resulting from applying a simple shear in the xz component (lines labeled with the appropriate model parameters). The dotted line shows the small strain approximation (12). An illustration of the elastomer is provided above the graph of the $(r,\theta)=(5,0.5^c)$ case.

tion for λ_{xx}. Whilst this quartic is soluble by radicals, the solution does not provide much insight. Some information about the nature of the solution can be gained by substituting $\lambda_{xx}=1+\epsilon$. Minimizing the resulting free energy with respect to ϵ results in

$$\epsilon = -\frac{(r-1)\lambda_{xz}\rho\sin(2\theta)}{1-(r-1)^2\cos 4\theta + r(r+30)}. \tag{12}$$

Note that ϵ is negative, i.e., the sample contracts along the direction of shear displacements. This is consistent with the imposed λ_{xx} behavior pointed out in the previous example. The modulus in this case is given by

$$\frac{4\rho^2}{\rho(r-\rho)+3r+\rho}\mu. \tag{13}$$

For large λ_{xz} (typically $\lambda_{xz}\sim 5$) it can be shown that the sympathetic λ_{xx} response behaves asymptotically as

$$\lambda_{xx} \sim \left[\frac{2r}{\lambda_{xz}(r-1)\rho\sin 2\theta}\right]^{1/3}. \tag{14}$$

The slope of the nominal stress-strain curve tends to

$$\frac{\rho^2}{r}\mu, \tag{15}$$

i.e., the sample always hardens as it is stretched. This result can be related to the stiffness of the sample when stretched along the **z** axis, calculated in the next section. An illustration of this behavior is shown in Fig. 4

If the layer normal and director are not fixed, then the sample simply rotates, since a λ_{zx} component necessarily has to be introduced into the deformation gradient.

Experimentally this deformation is difficult to apply because the region around the clamps must not contract. It is also observed that the sample starts to buckle when large shears are applied to it. However, the above example is important in the analysis of an imposed λ_{zz} because, by multiplication of suitable rotation matrices, the two problems can be related to one another, as we will now show.

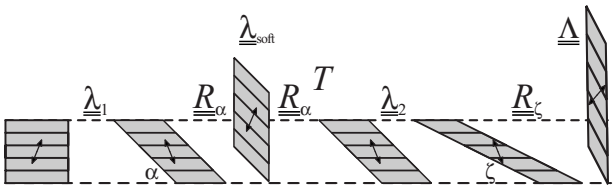

FIG. 5. Sequence of gedanken shears and rotations to achieve the maximal soft distortion ($\underline{\underline{\lambda}}_{soft}$) in response to z stretch, and then subsequent nonsoft distortion to attain a final $\underline{\underline{\Lambda}}$.

C. Imposed λ_{zz}

In this case the elastomer is initially soft, which complicates the analysis here. Soft modes in response to imposed λ_{zz} have been analyzed in detail elsewhere [6,9]; here we first look for the end of the soft mode as a starting point for the analysis. Note that the soft mode of a Sm-C elastomer in this geometry contrasts to the response of a Sm-A elastomer which has a very high modulus when stretched parallel to the **z** direction, followed by an abrupt change in elastic modulus from B to $r\mu$ due to the transition from stretching the layers to shearing them [5].

The first question addressed here is that of the final position of the director after the soft mode has ended. In general one would take the direction along which the elastomer is being stretched, **p** (here **z**), and then maximize the quantity $\mathbf{p}\cdot\underline{\underline{R}}\cdot\underline{\underline{\lambda}}(\xi)\cdot\mathbf{p}$, where $\underline{\underline{R}}$ is a rotation matrix and $\underline{\underline{\lambda}}(\xi)$ is one of the soft modes of the form $\underline{\underline{\lambda}}(\xi)=\underline{\underline{\ell}}_{\mathbf{n}}^{1/2}\cdot\underline{\underline{\ell}}_0^{-1/2}$, where **n** lies on the intersection of the unit sphere and a plane as described in [9]. In the geometry currently under consideration, there is a concrete sequence of gedanken deformations that this maximal soft stretch along **z** can be broken down into; see Fig. 5. Since in-plane shear is essentially the only soft deformation for Sm-C,it is clear that to obtain low cost deformation, the director must rotate through π about **z** from its initial condition to the final state, as illustrated in Fig. 1 and as $\underline{\underline{\lambda}}_1$ in Fig. 5. (The sphere mentioned above is one with the original layer normal defining a north pole, and the plane is that such that the circle of intersection with the sphere is the locus of **n** making angle θ with $\mathbf{k}_0$.) This in-plane soft deformation is given [9] by

$$\underline{\underline{\lambda}}_1 = \begin{pmatrix} 1 & 0 & -\dfrac{(r-1)\sin 2\theta}{\rho} \\ 0 & 1 & 0 \\ 0 & 0 & 1 \end{pmatrix} \quad \underline{\underline{R}}_\alpha = \begin{pmatrix} \cos\alpha & 0 & -\sin\alpha \\ 0 & 1 & 0 \\ \sin\alpha & 0 & \cos\alpha \end{pmatrix}. \tag{16}$$

Then to have achieved elongation along the extension direction z, one must apply a subsequent body rotation $\underline{\underline{R}}_\alpha$ (with axis parallel to **y**) to the distorted body. It rotates the sheared solid to the vertical position (Fig. 5 after $\underline{\underline{R}}_\alpha$). Thus an initial z segment of the body clearly achieves its maximal soft λ_{zz} component, stretch along z. The rotation must be by the same

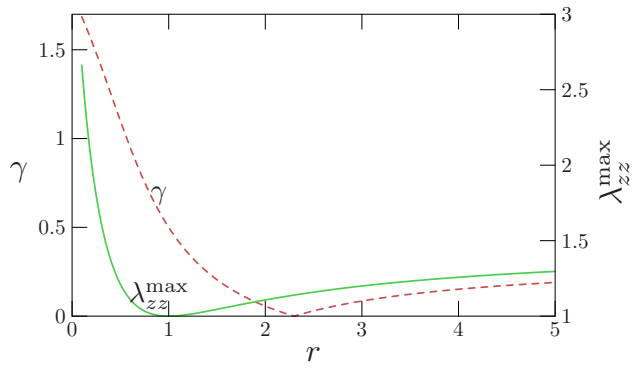

FIG. 6. (Color online) Extent of the soft mode $\lambda_{zz}^{\max}$ and the final angle of the director to the **z** direction at the end of the soft mode as a function of the anisotropy, r, for $\theta=0.5^c$.

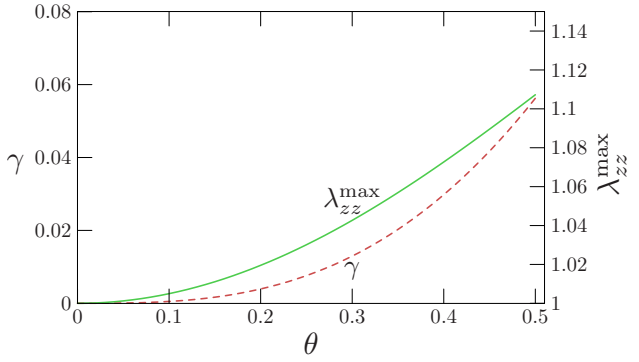

FIG. 7. (Color online) Extent of the soft mode $\lambda_{zz}^{\max}$ and the final angle of the director to the **z** direction at the end of the soft mode as a function of the molecular tilt, θ, for $r=2$.

angle α as the soft shear angle, but in the opposite sense

$$\tan\alpha = -\frac{(r-1)}{\rho}\sin 2\theta. \tag{17}$$

The maximal soft deformation matrix for the system when stretched parallel to the z axis is thus

$$\underline{\underline{\lambda}}_{\text{soft}} = \underline{\underline{R}}_{\alpha}\cdot\underline{\underline{\lambda}}_{1} = \begin{pmatrix} \frac{\rho}{\sqrt{\rho^2+(r-1)^2\sin^2 2\theta}} & 0 & 0 \\ 0 & 1 & 0 \\ -\frac{(r-1)\sin 2\theta}{\sqrt{\rho^2+(r-1)^2\sin^2 2\theta}} & 0 & \frac{\sqrt{\rho^2+(r-1)^2\sin^2 2\theta}}{\rho} \end{pmatrix}.$$

Rotation has eliminated the shear λ_{xz} in $\underline{\underline{\lambda}}_1$ in favor of the other shear λ_{zx} in $\underline{\underline{\lambda}}_{\text{soft}}$. Also apparent is that the soft mode ends when the stretch along the **z** direction is

$$\lambda_{zz} = \sqrt{1+\frac{(r-1)^2\sin^2 2\theta}{\rho^2}}. \tag{18}$$

Given that the body rotation α convects everything with it, the angle of the director to the z axis simply becomes

$$\gamma = \theta - \arctan\left[\frac{(r-1)}{\rho}\sin 2\theta\right] \equiv \theta+\alpha. \tag{19}$$

This angle is small for typical material parameters: for $\theta\sim 25°$ and $r\sim 2$, then $\gamma=3.24°$ which happens to be near the $r\approx 2.2$ where γ vanishes (i.e., where the shear angle can be identified with the tilt angle). In general it is not zero, so the director is not in general aligned with the z axis. The reason for the difference between the orientation of the director and the stretch axis is another manifestation of the difference between the director angle observed in x-ray scattering, θ_X and the tilt of the elastomer under shear θ_E, as shown theoretically in [8,15], and experimentally in [12].

An illustration of the angle between the stretch direction and the director and the extent of the soft mode as a function of the anisotropy, r is shown in Fig. 6. The same quantities as a function of the tilt angle, θ are shown in Fig. 7. These analytical predictions have been tested by minimization of the free energy density numerically, using the simplex algorithm.

The route taken to this final state can be calculated numerically by using a lower triangular deformation matrix. The form of this matrix is enough to uniquely determine the soft mode. Inclusion of upper triangular elements serve to make the soft mode nonunique by allowing rotation of the sample about additional axes. The free energy can be minimized directly by using the simplex algorithm. The director loops around on the surface of a sphere so as to maximize the extent of the soft mode along the **z** direction (Fig. 8). Note that during the soft mode the director, **n**, the layer normal, **k**, and the stretch direction, **z**, are not coplanar. At the end of the soft mode the three vectors are coplanar, and the director lies in the xz plane. The subsequent sympathetic shears, which are consequently reduced to just one off-diagonal element, are now calculated.

We now return to the simple scheme for envisaging deformation employed to find the soft mode. Deformation con-

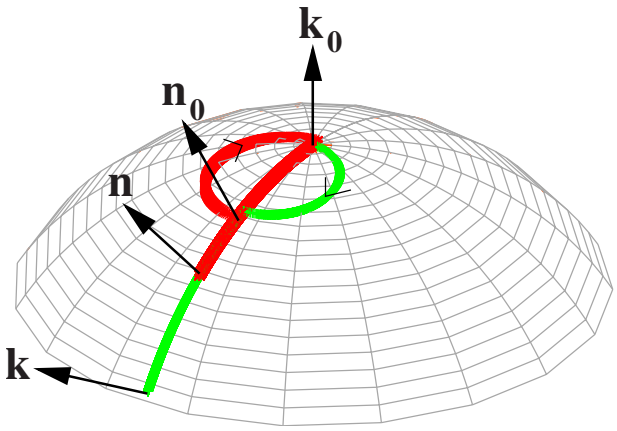

FIG. 8. (Color online) Path of the director (dark gray/red) and the layer normal (light gray/green) when the Sm-*C* elastomer is stretched parallel to the layer normal. The sample in this case has $r=2$ and $\theta=0.5^c=28.6°$. It is plotted up to $\lambda=2$ here, and the soft mode ends at $\lambda_{zz}\approx 1.3$. The arrows on the paths indicate the direction in which they are traversed as λ_{zz} is increased.

tinues to be effectively shear and stretch in-plane which we will again achieve via gedanken distortions and rotations. We take the total deformation tensor from the initial state to be

$$\underline{\underline{\Lambda}} = \begin{pmatrix} \Lambda_{xx} & 0 & 0 \\ 0 & \Lambda_{yy} & 0 \\ \Lambda_{zx} & 0 & \Lambda_{zz} \end{pmatrix}, \tag{20}$$

where $\Lambda_{xz}=0$ since displacements in the x direction while applying a σ_{zz} stress leads to torques that counter the displacement. Such shears are absent in deformations of nematic elastomers for the same reasons [2]. After the soft mode has finished then the deformation can be decomposed as follows in the limit $B/\mu \to \infty$

$$\underline{\underline{\Lambda}} = \underline{\underline{R}}_{\zeta} \cdot \underline{\underline{\lambda}}_2 \cdot \underbrace{\underline{\underline{R}}_{\alpha}^{T} \cdot \underline{\underline{\lambda}}_{\text{soft}}}. \tag{21}$$

The combination $\underline{\underline{R}}_{\alpha}^{T} \cdot \underline{\underline{\lambda}}_{\text{soft}}$ is just the original in-plane soft deformation $\underline{\underline{\lambda}}_1$, see Fig. 5, since a counter rotation, $\underline{\underline{R}}_{\alpha}^{T} \equiv \underline{\underline{R}}_{-\alpha}$ has acted. A further (now hard) in-plane shear and stretch (with volume conservation), $\underline{\underline{\lambda}}_2$, is then applied (since these modes leave the layer spacing untouched):

$$\underline{\underline{\lambda}}_2 = \begin{pmatrix} \lambda_{xx} & 0 & \lambda_{xz} \\ 0 & 1/\lambda_{xx} & 0 \\ 0 & 0 & 1 \end{pmatrix}. \tag{22}$$

Thus, in this decomposition, the sheared state of Eq. (16), the end of the in-plane soft deformation, is stretched in the **x** direction and sheared in the xz plane. The operations of Eq. (22) are elementary ones of Figs. 2(a) and 2(b), see also Fig. 5. The body is then rotated about the **y** axis by $\underline{\underline{R}}_{\zeta}$ to reach the final state in such a way that xz shear is eliminated in the final state. The angle ζ is not, as before, simply the inverse tangent of the shear since we have elongation λ_{xx} at the intermediate step $\underline{\underline{\lambda}}_2$ and since we are dealing with finite distortions, they compound in a nonlinear way rather than simply adding.

By equating the Λ_{xz} component to zero it follows that the required rotation angle ζ is

$$\tan\zeta = \lambda_{xx}\frac{(r-1)}{\rho}\sin 2\theta - \lambda_{xz} \tag{23}$$

and thus

$$\Lambda_{xx} = \frac{\lambda_{xx}}{\sqrt{1+\tan^2\zeta}}, \tag{24}$$

$$\Lambda_{yy} = \frac{1}{\lambda_{xx}}, \tag{25}$$

$$\Lambda_{zz} = \sqrt{1+\tan^2\zeta}, \tag{26}$$

$$\Lambda_{zx} = -\frac{\lambda_{xx}\tan\zeta}{\sqrt{1+\tan^2\zeta}}. \tag{27}$$

It can then be deduced that

$$\Lambda_{yy} = \frac{1}{\Lambda_{xx}\Lambda_{zz}}, \tag{28}$$

$$\Lambda_{zx} = -\Lambda_{xx}\sqrt{\Lambda_{zz}^2 - 1}. \tag{29}$$

The angle of the layer normal to the z axis can also be determined

$$\tan\zeta = \sqrt{\Lambda_{zz}^2 - 1}, \tag{30}$$

from which the director angle follows by subtracting θ.

Using Eq. (26) and Eq. (23) to fix the λ_{xz} component in terms of Λ_{zz} and λ_{xx}, then the resulting effective simple shear and elongation applied to the sample is

$$\underline{\underline{\lambda}} = \begin{pmatrix} \lambda_{xx} & 0 & -\sqrt{\Lambda_{zz}^2 - 1} + \lambda_{xx}\dfrac{(r-1)}{\rho}\sin 2\theta \\ 0 & 1/\lambda_{xx} & 0 \\ 0 & 0 & 1 \end{pmatrix},$$

where the λ_{xx} component has been mixed into the xz entry. The components of this deformation tensor can be substituted into the free energy density given in Eq. (7) resulting in

$$f = \tfrac{1}{2}\mu\left(\lambda_{xx}^2 + \frac{1}{\lambda_{xx}^2} + 1 + \frac{1}{r}\left[\rho\sqrt{\Lambda_{zz}^2 - 1} + \tfrac{1}{2}(1+\lambda_{xx})(r-1)\sin 2\theta\right]^2\right). \tag{31}$$

After the soft mode [when Λ_{zz} is greater than the expression of Eq. (18)], then λ_{xx} deviates from 1.

Asymptotically the nominal stress on the z face required to extend the elastomer tends to

$$\sigma \sim \mu(\rho^2/r)\Lambda_{zz}. \tag{32}$$

This expression reduces to that of the Sm-A elastomer for $\theta=0$, and is also similar to the asymptotic modulus given for the xz shear in the previous section.

The threshold that was observed in the Sm-A case is clearly no longer present in the Sm-C elastomer. This is illustrated in Fig. 9, which shows numerical calculation of four nominal stress strain curves, again using the simplex algorithm, for different tilt angles of the director and anisotropies of the polymer chain distribution. The stress strain curves show first a soft plateau at zero stress and then a singular rise in the stress as the sample begins to deform by shearing the smectic layers.

IV. POLYDOMAIN ALIGNMENT

Since liquid crystal elastomers were first fabricated, construction of monodomain samples (single crystals) has been important experimentally so that, for example, the elastic properties of the material are not obscured by the effects of the polydomain-monodomain transition. In nematic elastomers the two principal methods of alignment are by applying a strong magnetic field during crosslinking [16], or employing a two stage crosslinking process, whereby the sample is initially weakly crosslinked and then a second

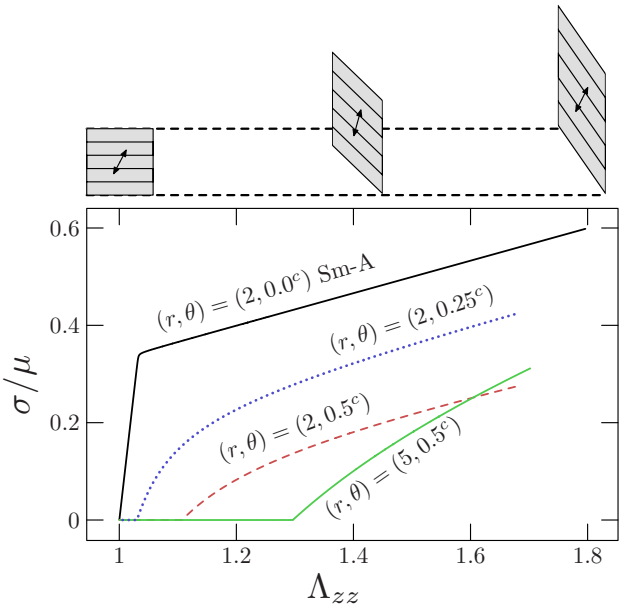

FIG. 9. (Color online) Four nominal stress-strain curves for an elastomer with $B/\mu=60$, (r,θ) given on the relevant lines. An illustration of the elastomer is provided above the graph of the $(r,\theta)=(5,0.5^c)$ case.

crosslinking stage is carried out with the sample under a load [17]. For liquid crystal phases with more complicated order such as the cholesteric and smectic phases, a more involved alignment process has been developed. For Sm-*A* systems, a two-stage crosslinking procedure is carried out, just as for the nematic case, but during the final stage the aligned sample is cooled into the smectic state. In Sm-*C* elastomers it is particularly difficult to obtain a monodomain, because of the angle between the layer normal and the director. If the sample undergoes a second crosslinking whilst under uniaxial load, then a chevron microstructure results [18]. Two ways of applying a mechanical deformation to obtain an Sm-*C* monodomain have been reported. A second uniaxial elongation can be applied to the chevron structure at a specified angle to the layer normal. This has the effect of removing all but one of the layer orientations [19]. Another method is to apply a shear deformation to the chevron texture, which again has the effect of selecting out a particular orientation for the layer normal [20]. Here we look at the effect of uniaxial deformations and shears on a collection of domains to see if the applied deformation can align the directors.

A. Alignment by uniaxial extension

This method of formation of monodomains was employed experimentally in [19], where a sample was reoriented using a secondary elongation $\lambda_2=1.6$. The geometry of this method is indicated in Fig. 10. To investigate this method of alignment, the effects of a uniaxial elongation on a collection of domains treated independently and with the orientations of director and layer normal as shown in Fig. 10 was investigated. The layer normals, **k**, sit on a cone about the common

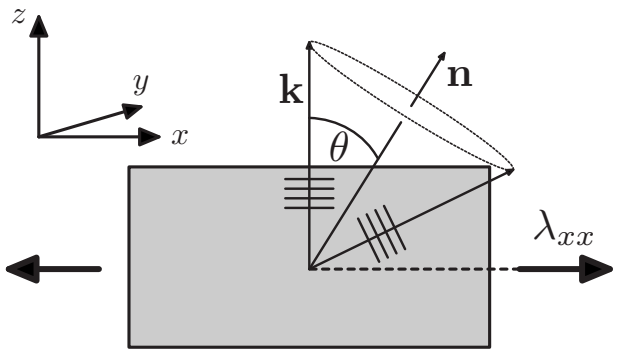

FIG. 10. Polydomain Sm-*C* elastomer with aligned directors as shown, but with all possible layer normals that maintain the correct tilt angle with respect to the director. The polydomain is aligned by stretching perpendicular to a particular layer normal as shown, that is at an angle of $90°-\theta$ to **n**.

director **n**. The deformation gradient used was a lower triangular matrix

$$\underline{\underline{\lambda}} = \begin{pmatrix} \lambda_{xx} & 0 & 0 \\ \lambda_{yx} & 1/(\lambda_{xx}\lambda_{zz}) & 0 \\ \lambda_{zx} & \lambda_{zy} & \lambda_{zz} \end{pmatrix}, \tag{33}$$

where the Cartesian axes are as shown in Fig. 10. Note that this matrix would not be permitted for a monodomain with an imposed λ_{xx} as discussed in Sec. III. However, because we are considering a domain within a polydomain sample more freedom in the deformation gradient has been included. The λ_{xx} component was then imposed and the remaining elements and the angle of the **c** vector in the plane perpendicular to **k** minimized numerically, using the simplex algorithm. The results projected onto the *xy* plane are shown in Fig. 11. Note that the paths of the director move around on closed loops, whereas the layer normals are all attracted towards the **z** axis. The robustness of this result was checked by reducing the number of elements in the deformation gradient that are minimized over. The results do change markedly depending on which of the elements $(\lambda_{yx},\lambda_{zx},\lambda_{zy},\lambda_{zz})$ are permitted to relax. If one of these elements was constrained then the layer normal quickly reaches the *xz* plane, but takes some time to move up to the **z** direction. However, if two or more elements were constrained then the results change drastically. The layer normal moves towards the **y** direction, and the director position is broadly distributed around this direction. This dependence should be explored further in a more detailed model of polydomain reorientation.

Typically, rather large strains were required to realign the system, approximately $\lambda=8$ or more. This is considerably more than those reported in [19]. It is also larger than the strain of $\lambda=4$ reported in [21] to untwist a helical superstructure by a uniaxial strain in a smectic-C^* elastomer. The discrepancy between these results may be explained by the additional constraints on neighbouring domains in the polydomain due to compatibility. Alternatively, a microscopic redistribution of the macroscale strain may occur as

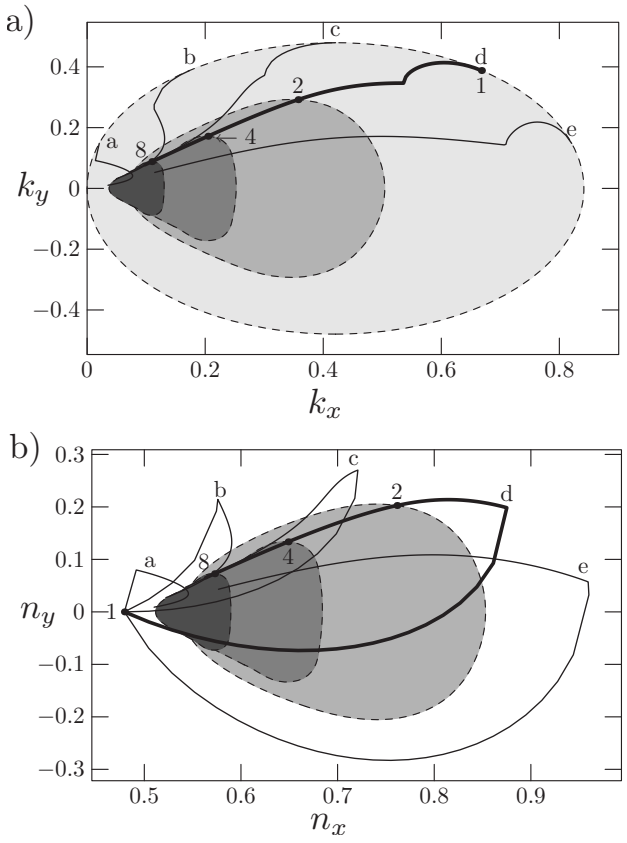

FIG. 11. (a) Paths of the layer normal and (b) paths of the director projected onto the xy plane, as the system is realigned. The value of the deformation λ_{xx} along a particular path is marked, and contours of equal λ_{xx} highlighted. Corresponding paths in each figure are labeled a–e. Here $r=2$, $\theta=0.5^c$, and $B=60$.

the polydomain is elongated. The domains that are close to the fully aligned state take up a much smaller fraction of the macrostrain than the neighbouring domains that are further from being in the fully aligned state. The latter deform at lower energy cost and in taking a larger fraction of the macrostrain suffer much larger microscopic (local) strains.

B. Alignment by simple shear

1. Experimental geometry

Shearing polydomain samples using a rigid frame has used experimentally to construct monodomains in [20]. This is a two stage crosslinking process where a shear angle of around 30° (=arctan λ_{xz}) is applied before the second crosslinking, corresponding to a simple shear of $\lambda_{xz}\sim 0.5$, followed by an annealing cycle. Here the initial distribution of layer normals is shown in Fig. 12. In this example it was possible to use a much more constrained deformation gradient: $\underline{\underline{\lambda}}=\underline{\underline{\delta}}+\lambda_{xz}\mathbf{xz}$, only minimizing over the angle of **c** perpendicular to the director.

Since the effect of the shear deformation is rotation about the y axis it was found that half of the layer normals rotate to the north pole on the unit sphere, and half to the south pole. We illustrate the two halves separately here.

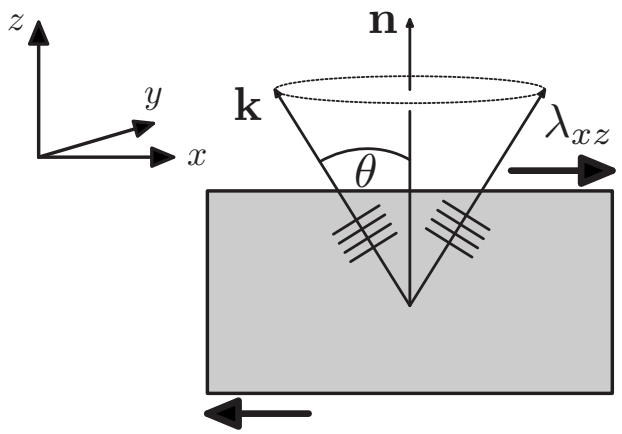

FIG. 12. Polydomain Sm-C elastomer with aligned directors as shown, with all possible layer normals on a cone that maintain the correct tilt angle with respect to the director. The polydomain is aligned by shearing perpendicular to the director as shown.

The paths of the layer normals to the north pole are shown in Fig. 13(a). We again see in this figure the large values of the deformation required in this approximation to align the monodomains. Ultimately the layer normals are all migrating to the north pole, with the directors tilted toward the **x** direction.

The longer paths of the layer normals to the south pole are shown in Fig. 13(b). The associated director paths are far more complicated, but eventually end up tilted along the **−x** direction. The symmetry of the director and layer normal (

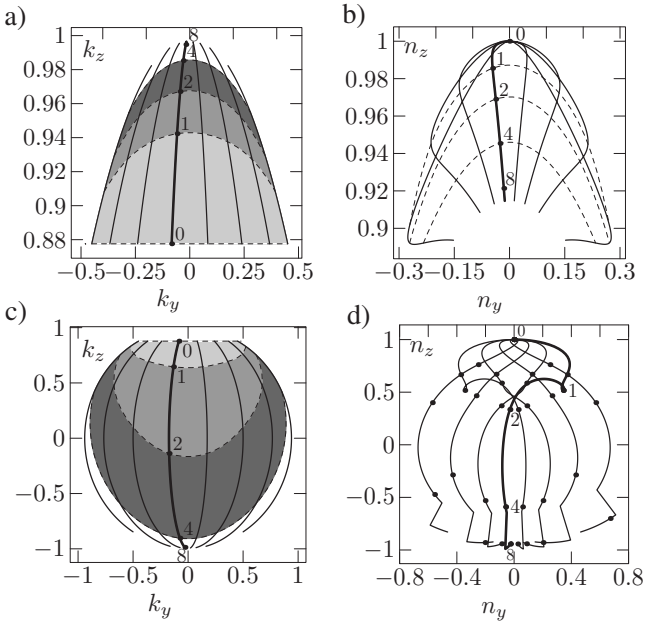

FIG. 13. Paths of the layer normal and director, respectively, projected onto the yz plane, as the system is realigned by a shear deformation indicated in Fig. 12, (a) **k** to north pole, (b) corresponding reorientation of **n**, (c) **k** to south pole, and (d) corresponding reorientation of **n**. The value of the deformation λ_{xz} along a particular path is marked. Here $r=2$, $\theta=0.5^c$, and $B=60$.

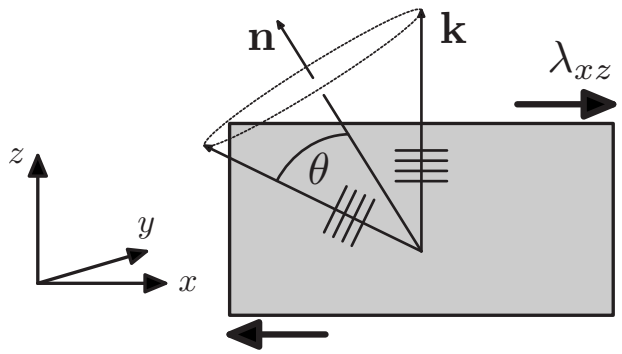

FIG. 14. Polydomain Sm-*C* elastomer with aligned directors as shown, but with all possible layer normals on a cone that maintain the correct tilt angle with respect to the director. The polydomain is aligned by shearing perpendicular to the layer normal as shown.

n→−**n** and **k**→−**k**) dictates that the north pole and south pole populations, and their associated directors are equivalent. Note that the discontinuity in the director path in Fig. 13(b) occurs because the directors jump from n_x to $-n_x$ in order to reach their final position.

Whilst the layer normals can respond here without the need for sympathetic shears, the division of the population into two halves may explain the need to anneal the sample experimentally to obtain monodomains.

2. Alternative geometry

The problems of the geometry described in the previous section can be avoided by changing the geometry of the shear performed, as illustrated in Fig. 14. This geometry has the advantage that some of the domains can deform softly, and that all of the layer normals are swept to the north pole on the unit sphere. An illustration of the realignment from the deformation gradient $\underline{\underline{\lambda}}=\underline{\underline{\delta}}+\lambda_{xz}\mathbf{xz}$ is shown in Fig. 15. It can be seen from the figure that those domains that are soft reach full alignment extremely quickly, in a shear of less than 1, whereas those requiring a large movement of the layer normal again have to undergo extensive shearing to reach the aligned position.

V. DISCUSSION

The calculations presented in this paper based on modelling a Sm-*C* elastomer as a nematic with embedded layers and with restricted director motion suggest many interesting experiments. However, even without soft elasticity, the elastic behavior of Sm-*C* elastomers has rich behavior, with the possibility of complex microstructures if rigid clamps are used to impose deformations. In other liquid crystal elastomer systems it has been observed that whilst the formation of a microstructure may affect for example the birefringence of the sample dramatically, it does not much increase the elastic stiffness. We anticipate a similar behavior in this system. The soft modes permitted by the formation of microstructure have been analysed in Ref. [13], where it is proven that stretching parallel to the layer normal is not a soft deformation because of the restriction of the compatibility of the microstructures. An experimental test of soft elasticity, and the associated microstructure have also been suggested in Ref. [13].

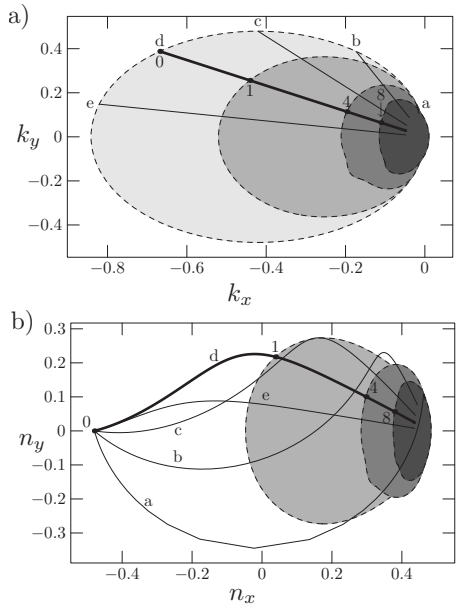

FIG. 15. (a) Paths of the layer normals and (b) paths of the director projected onto the *xy* plane, as the system is realigned in the geometry of Fig. 14. The value of the deformation λ_{xz} along a particular path is marked, and contours of equal λ_{xz} are highlighted. Corresponding paths in each figure are labeled *a*–*e*. Here $r=2$, $\theta=0.5^c$, and $B=60$.

The analysis of the aligning polydomain samples shows that the model used here is consistent with the experimental procedures of aligning Sm-*C* polydomains. However, it does raise the question of why such large deformations are required in comparison to experimental alignment. It also illustrates a problem, in theory at least, with the current geometry of the shear induced alignment: The population of layer normals is split into two.

It is well known that the low symmetry of the Sm-*C* phase allows a polarization direction to be defined from the cross product of **n** and **k**. The deformations reported in Secs. III A and III B do not change the orientation of the polarization. The polarization is rotated in the soft part of the deformation of Sec. III C, but remains invariant after the soft mode has finished. The piezoelectric properties are thus intimately related to the soft deformation, where large reorientations of the director and layer normal occur. These reorientations also occur in the polydomain deformations considered in Sec. IV.

VI. CONCLUSIONS

The three deformations considered in Sec. III illustrate how a Sm-*C* elastomer responds to a variety of deformations. The initial soft response is a consequence of the freedom of the director, which can rotate around the layer normal. After the sample reaches its maximum soft extension the director then has no freedom and is a slave of the layer normal. The

response of the Sm-*C* elastomer is then principally due to the reorientation of the layer normal away from the direction of maximum elongation. Once the soft mode has been extracted, the only distinct deformations that the elastomer can undergo are elongations perpendicular to the layer normal, and shears perpendicular to the layer normal. An example of how a deformation can be decomposed was given in Sec. III C.

Various testable experimental predictions can be made of the theory in this paper, for example on stretching a monodomain parallel to the layer normal specific features of the stress strain curve can be calculated. The extent of the soft plateau is predicted by Eq. (18), as well as the asymptotic modulus of Eq. (32) and its equivalence to the asymptotic shear modulus in Eq. (15). Two values for asymptotic modulus for a uniaxial stretch perpendicular to the layer normal were predicted, depending on the freedom of the system to form microstructure.

The model of Sec. II was compared to experiments on the alignment of polydomain samples by calculating the response of the layer normal and director in a set of independent monodomains. The results are qualitatively consistent with the experimental alignment, however it was found that larger strains than reported experimentally are required. An alternative geometry for the alignment of Sm-*C* polydomains was also suggested in Sec. IV B 2.

ACKNOWLEDGMENTS

J.M.A would like to thank the Royal Commission for the Exhibition of 1851 and Fitzwilliam College for support.

[1] P. D. Olmsted, J. Phys. II **4**, 2215 (1994).
[2] M. Warner and E. M. Terentjev, *Liquid Crystal Elastomers* (Oxford University Press, Oxford, 2007).
[3] L. Golubovic and T. C. Lubensky, Phys. Rev. Lett. **63**, 1082 (1989).
[4] E. Nishikawa and H. Finkelmann, Macromol. Chem. Phys. **198**, 2531 (1997).
[5] J. M. Adams and M. Warner, Phys. Rev. E **71**, 021708 (2005).
[6] O. Stenull and T. C. Lubensky, Phys. Rev. E **76**, 011706 (2007).
[7] O. Stenull and T. C. Lubensky, Phys. Rev. Lett. **94**, 018304 (2005).
[8] O. Stenull and T. C. Lubensky, Phys. Rev. E **74**, 051709 (2006).
[9] J. M. Adams and M. Warner, Phys. Rev. E **72**, 011703 (2005).
[10] A. S. Merekalov, S. A. Kuptosov, G. A. Shandryuk, R. V. Talroze, V. S. Bezborodov, and E. M. Terentjev, Liq. Cryst. **28**, 495 (2001).
[11] A. Sanchez-Ferrer and H. Finkelmann, Macromolecules **41**(3), 970 (2008).
[12] K. Hiraoka, W. Sagano, T. Nose, and H. Finkelmann, Macromolecules **34**, 7352 (2005).
[13] J. Adams, S. Conti, and A. DeSimone, Continuum Mech. Thermodyn. **18**, 319 (2007).
[14] E. Nishikawa and H. Finkelmann, Macromol. Chem. Phys. **200**, 312 (1999).
[15] J. M. Adams and M. Warner, Phys. Rev. E **73**, 031706 (2006).
[16] C. H. Legge, F. J. Davis, and G. R. Mitchell, J. Phys. II **1**, 1253 (1991).
[17] J. Kupfer and H. Finkelmann, Makromol. Chem., Rapid Commun. **12**, 717 (1991).
[18] K. Hiraoka, Y. Uematsu, P. Stein, and H. Finkelmann, Macromol. Chem. Phys. **203**, 2205 (2002).
[19] K. Semmler and H. Finkelmann, Macromol. Chem. Phys. **196**, 3197 (1995).
[20] K. Hiraoka and H. Finkelmann, Macromol. Rapid Commun. **22**, 456 (2001).
[21] R. Zentel, Liq. Cryst. **3**, 531 (1988).